Damage-induced basal epithelial cell migration modulates the spatial organization of redox signaling and sensory neuron regeneration

Alexandra M. Fister[1, 2, §], Adam Horn[1, §], Michael Lasarev[3], and Anna Huttenlocher[1, 4, *]

[1]Department of Medical Microbiology and Immunology, University of Wisconsin-Madison, Madison, United States.

[2]Cellular and Molecular Biology Graduate Program, University of Wisconsin-Madison, Madison, United States.

[3]Department of Biostatistics and Medical Informatics, University of Wisconsin-Madison, Madison, United States.

[4]Department of Pediatrics, University of Wisconsin-Madison, Madison, United States.

[§]These authors contributed equally.

[*]Corresponding Author: huttenlocher@wisc.edu

Summary

Epithelial damage leads to early reactive oxygen species (ROS) signaling, which regulates sensory neuron regeneration and tissue repair. How the initial type of tissue injury influences early damage signaling and regenerative growth of sensory axons remains unclear. Previously we reported that thermal injury triggers distinct early tissue responses in larval zebrafish. Here, we found that thermal but not mechanical injury impairs sensory axon regeneration and function. Real-time imaging revealed an immediate tissue response to thermal injury characterized by the rapid Arp2/3-dependent migration of keratinocytes, which was associated with tissue-scale ROS production and sustained sensory axon damage. Osmotic regulation induced by isotonic treatment was sufficient to limit keratinocyte movement, spatially-restrict ROS production and rescue sensory function. These results suggest that early keratinocyte dynamics regulate the spatial and temporal pattern of long-term signaling in the wound microenvironment during tissue repair.

Introduction

Restoration of tissue function following epithelial injury requires the regeneration and activity of peripheral sensory neurons, which innervate the skin[1–3]. In response to tissue damage, sensory neurons undergo rapid and localized axonal degeneration[4,5]. The process of axonal regeneration first requires the clearance of axon fragments by phagocytes followed by new axonal growth[6]. While peripheral sensory neurons maintain a cell-intrinsic ability to regenerate following injury[7–9], local environmental cues also regulate the response of sensory neurons to tissue damage *in vivo*. Recent advances have identified the contribution of supporting cell populations, paracrine biochemical signaling, and biophysical interactions in regulating peripheral sensory axon regeneration[10–12]. Despite these advances, we have limited understanding of how early collective signaling in the wound microenvironment is organized and leads to sensory axon regeneration and tissue repair.

Epidermal keratinocytes are a primary constituent of epithelial tissue and play a critical role in wound healing. In addition to mediating wound closure by actively migrating toward the site of injury, keratinocytes also generate pro-reparative signals such as reactive oxygen species (ROS), which coordinate longer-term repair pathways [13–19]. While transient and localized ROS production promote regeneration and sensory neuron regrowth, chronically elevated ROS are associated with neurodegeneration and disease[17,20,21]. Thus, precise temporal and spatial organization of tissue redox signaling is likely critical for efficient sensory neuron regeneration and tissue repair.

While epithelial tissue is well-adapted to repair from mechanical damage, burn wounds heal poorly. Thermal injury results in chronic pain and lack of sensation, suggesting that an abnormal sensory neuron response contributes to burn wound pathophysiology [22–26]. Despite this, we lack an understanding of why sensory neuron function is impaired after burn. Our previous work has demonstrated persistent inflammation and a loss of an organized collagen matrix that impairs healing after thermal injury in larval zebrafish[27–29]. These features recapitulate human burns and provide an *in vivo* model system to study the regeneration of sensory neurons in the wound microenvironment.

Using real time imaging, we took advantage of the optical transparency of larval zebrafish to dissect dynamic cell-cell interactions in the wound microenvironment following injury. We found that localized thermal injury induced substantial axonal damage in the tail fin. Live imaging revealed that sensory axons are physically displaced and experience damage associated with rapid collective migration of basal keratinocytes following burn. This early keratinocyte migration also contributes to elevated ROS at the tissue-scale. Keratinocyte migration was dependent on Arp2/3 signaling and inhibition with CK666 restored early wound-localized ROS production after injury, suggesting that dysregulated migration perturbs the temporal and spatial organization of ROS after tissue damage. Inhibiting keratinocyte migration via osmotic manipulation spatially restricted ROS production and rescued sensory axon regrowth and function. Osmotic modulation did not restore sensory axon regrowth if the treatment was started after keratinocyte migration had occurred. Collectively, our results support the importance of regulated keratinocyte behavior for early temporal and spatial signal control that leads to sensory axon regeneration and tissue repair.

Results

Burn injury increases peripheral sensory axon damage

To visualize sensory neurons responding to tissue injury, we used 3 days post-fertilization (dpf) *Tg(Ngn1:GFP-Caax)* larval zebrafish that express GFP in sensory neurons[30–32]. Larvae were either mechanically injured by tailfin transection or burn as previously described (**Fig. 1A**)[27]. Intravital imaging of larvae beginning at 24 hours post wound (hpw) revealed an abnormal axon morphology in burned larvae compared to mechanical transection, with axons showing fewer branch points (**Fig. 1B**). To evaluate sensory axons following injury, we assessed axon density in the wounded tissue posterior to the notochord 24 hpw. Larval zebrafish caudal fins can regenerate fully by 3 days post-transection, with 60% of fin regrowth occurring by day 1.5[33]. Following transection, axon density was 89.5 ± 0.02% of the density observed in age-matched uninjured larvae 24 hpw. In contrast, we found that burned larvae had significantly impaired sensory axon density, with an axon density of 63.7 ± 0.02% compared to uninjured fins (**Fig. 1C**). This relative decrease was

sustained even 96 hours post burn (hpb) with an axon density of only 65.1 ± 0.04% compared to control (**Fig. 1C**). To test whether this regenerative defect was associated with a defect in sensory neuron function, we assessed the touch responsiveness of wounded tissue. Light pressure was applied by an eyelash brush directly to the wound area, and sensory neuron function was scored by the presence of a tail flick reflex[34]. As expected, larvae wounded by transection had a nearly 100% response rate 24 hpw, highlighting the rapid recovery of sensory neurons following mechanical injury (**Fig. 1D**). In contrast, none of the burned larvae were sensitive to touch 24 hpb with resolution only occurring by 96 hpb (**Fig. 1D**). Importantly, all tested larvae exhibited a tail flick reflex when pressure was applied to the trunk, demonstrating that impaired sensation was limited to the damaged tissue.

We next sought to further investigate sensory neuron function in burned tissue. For this, we assessed wound-induced axonal damage using zebrafish larvae that express the calcium probe GCaMP. As shown previously by other groups, GCaMP labels degenerating neurons in real time[35]. Axon degeneration is characterized by damaged processes fragmenting and forming small punctae, which are later cleared by phagocytes[4,10]. While calcium increase following axonal damage is required for immediate membrane repair and subsequent regeneration, chronically elevated cytosolic calcium is associated with cell death and degeneration[36]. Therefore, imaging of neuronal calcium flux enables real-time labeling of axon damage in larval zebrafish[37–39]. Using *Tg(Elavl3:GCaMP5)* larvae, we observed minimal calcium flux under homeostatic conditions. However, the neurotoxin sodium azide elicited widespread and long-lasting calcium-positive punctae, indicating sustained axonal damage (**Fig. S1A**)[37]. Unlike Ngn1, the Elavl3 promoter is expressed by both sensory and motor neurons. To ensure that the calcium increase in epithelial tissue was specific to sensory neurons, sensory neurons were depleted by injecting Ngn1 morpholino into Elavl3:GCaMP5-expressing embryos. As expected, no calcium increase was detected in Ngn1 depleted larvae following injury (**Fig. S1B**). Time-lapse images were taken of Elavl3:GCaMP5 larvae to visually capture instances of axon damage leading to calcium-positive punctae, which occurs over the span of 30 minutes (**Fig. S1C**). These were compared to time-lapse images of sensory neuron-labeled larvae to verify damage occurs similar to Elavl3:GCaMP5 larvae, as evidenced by punctae formation over the span of 30 minutes (**Fig. S1D**). In agreement with previous

observations of axonal damage following mechanical injury[6,20,40], tailfin transection resulted in spatially localized axonal damage that was almost completely resolved by 1 hpw (**Fig. 1E**). In contrast, burn injury resulted in a distinct temporal and spatial profile of sensory axon damage. While initial wound-induced sensory neuron-specific calcium increase appeared to be localized to burned tissue, axonal damage continued to increase and spread across the tissue for approximately 6 hours (**Fig. 1E,F**). This raised the question of whether axonal damage was restricted to epithelial tissue directly impacted by injury, as observed in transected larvae. To label wounded epithelium, we used the lipophilic dye FM 1-43, which is commonly used to label damaged cell membranes after wound application[41–44]. Immediately following either transection or thermal injury, axonal damage overlapped spatially with wounded epithelial tissue (**Fig. 1G, H**). However, by 6 hpw, there was widespread damage to axons that extended beyond the initial wound area (**Fig. 1G, H**). These findings suggest that burn injury induces axonal damage that accumulates over time and is spatially uncoupled from the surrounding epithelial damage.

The burn wound microenvironment contributes to defective axon outcomes

To determine if early wound signaling regulates sensory neuron recovery, we used a two-wound model (**Fig. 2A**) to excise the burned tissue. In this system, zebrafish were first injured by either tailfin transection or burn and then a second transection injury was carried out either 5 minutes post-wound to allow for immediate signaling, or 6 hours post wound to coincide with the timing of peak axonal damage. The secondary transection was performed so that all the burned tissue was excised (**Fig. 2A, B**). As expected, larvae that underwent initial transection showed complete restoration of sensory function by 24 hpw, regardless of the timing of the secondary transection injury, highlighting the ability of zebrafish to efficiently heal from mechanical damage (**Fig. 2C-E**). In burned larvae, early transection after thermal injury restored sensory axon outcomes similar to transected tailfins when measured 24 hours after the second wound (**Fig. 2C-E**), suggesting that burn injury does not immediately affect sensory neurons differently than mechanical damage. However, when burned tissue was excised after 6 hours, we noted significant defects in both axon density and sensory function compared to larvae that received two transection injuries (**Fig. 2C-E**). These findings suggest that the local wound

environment modulates sensory axon outcomes following burn injury, and that events in the first 6 hours after injury impact longer term sensory axon repair.

Burn injury induces the collective movement of keratinocytes and sensory axons

To understand how burn injury damages sensory axons, we live imaged the behavior of keratinocytes, which closely associate with sensory axons[20,45,46]. Live-imaging of *Tg(Krt4:UtrCH-GFP)* larvae that express the actin probe Utrophin under a pan-keratinocyte promoter allowed for visualization of keratinocyte dynamics following either mechanical or burn injury. In response to transection, we initially observed characteristic epithelial cell contraction at the wound edge; however, keratinocytes distal to the wound edge remained relatively stationary (**Fig 3A; Supplemental Movie 1**). In contrast, burn wounding resulted in a rapid collective movement of keratinocytes toward the site of tissue damage (**Fig 3A; Supplemental Movie 1**). To quantify the rapid movement of keratinocytes in burn injured larvae, we used *Tg(Krtt1c19e:acGFP)* zebrafish to specifically label motile basal epithelial cells (**Fig. S2A**) [47–49]. Live-imaging experiments revealed that basal keratinocytes, on average, move a total distance of 205.7±10.7 µm in the first hour following burn injury, which was significantly greater than the 58.9±5.8 µm of migration observed following tailfin transection (**Fig 3B; Fig. S2A, B**). Although keratinocytes moved as a collective in response to burn injury, they exhibited chaotic movement and appeared to be loosely associated with their neighbors.

To determine if this process was due to active migration, time-lapse imaging was performed using *Tg(Krt4:Lifact-mRuby)* larvae to visualize the actin dynamics of both the superficial and basal layers. Unwounded larvae had regularly shaped and spaced keratinocytes with even actin distribution around the cell periphery in both the superficial and basal layers (**Fig. 3C**), indicative of a non-migratory epithelium. Superficial keratinocytes in burned larvae were elongated and had an even actin distribution, but the basal keratinocytes showed actin localization to the leading edge with the formation of lamellipodia (**Fig. 3C**), suggesting that the superficial keratinocytes are being pulled by the motile basal keratinocytes.

The axons of sensory neurons are ensheathed within actin-rich channels running through basal keratinocytes[50,51]. Given the chaotic and sustained keratinocyte migration associated with burn injury, we next

tested if sensory axons remain ensheathed within the motile basal keratinocytes. Simultaneous imaging of basal keratinocytes and sensory axons following thermal injury revealed that sensory axon movement is coordinated with keratinocyte migration (**Fig 3D; Supplemental Movie 2**). To determine the kinetics of axonal damage following burn, time lapse movies were performed with *Tg(Elavl3:GCaMP5)* larvae to identify if the onset of axonal damage occurs during basal keratinocyte migration. Within the first hour after burn, we identified calcium-positive punctae that coincided with keratinocyte migration, indicating that the early keratinocyte migration was associated with the initial axonal damage (**Supplemental Movie 3**). To determine if damage was limited to the axons, we imaged the cell bodies of peripheral sensory neurons. At 3 days post-fertilization, the skin is innervated by Rohon-Beard (RB) and dorsal root ganglia (DRG) neurons with cell bodies that reside within and just outside the spinal cord, respectively (**Fig. S1E**). Following burn injury, we noted that both the RB and DRG cell bodies were intact and non-motile in comparison to their pre-burn morphology (**Fig. S1E, F**). Taken together, these findings indicate that sensory axons and basal keratinocytes move as a collective following burn, and that this early movement is associated with the start of axonal damage.

The Arp 2/3 inhibitor CK666 impairs initial basal keratinocyte migration and modulates early ROS signaling following burn

To characterize the movement of keratinocytes after thermal injury, we determined if a known regulator of leading edge actin dynamics and migration, Arp2/3, modulates the movement of basal keratinocytes after burn[52]. Treatment with the Arp2/3 inhibitor CK666 limited keratinocyte lamellipodia formation, and impaired early keratinocyte migration, indicating that the early movement is Arp2/3 dependent [52] (**Fig. 4A-C**). Although early migration was impaired, by 40 minutes after burn the migration was not significantly different between control and CK666 treated larvae, suggesting that CK666 treatment only partially inhibits keratinocyte migration. To determine if this early treatment altered signaling in wounded tissue, we probed the effects of burn with and without CK666 treatment on the generation of reactive species (ROS) signaling at the wound. Efficient tissue repair after injury relies on coordinated ROS production by epithelial cells [53–55]. Following mechanical injuries such as tailfin transection or laser ablation, transient and localized H_2O_2 promotes sensory

axon regeneration and wound healing[20,56]. Because of this, we hypothesized that the excessive keratinocyte movement and sustained damage in burn tissue may result in dysregulated ROS production. To test this, H_2O_2 level was imaged using the fluorescent dye pentafluorobenzenesulfonyl fluorescein (Pfbsf). Early after burn wounding, there was robust generation of hydrogen peroxide in burned tissue that was dampened in CK666 treated larvae. In the presence of CK666 H_2O_2 production was concentrated at the wound edge, similar to what has been reported with tail transection, suggesting that early migration alters the temporal and spatial distribution of ROS after wounding (**Fig. 4D, E**). Although early ROS production was dampened, ROS production was increased both in the wound area and throughout the tailfin in CK666-treated larvae 6 hpw (**Fig. 4F, G**). In accordance with the elevated ROS level that developed later, CK666-treated larvae had no significant difference in axon damage or regeneration 24 hours after burn compared to controls, although there was a slight trend toward improvement (**Fig. 4H-J**). Taken together, the findings suggest that keratinocyte migration regulates early tissue scale ROS production after burn injury.

Keratinocyte movement induced by burn injury alters the temporal and spatial distribution of redox signaling

To determine if other treatments that affect keratinocyte migration also impact tissue scale ROS production after burn, we determined if osmotic modulation impacts keratinocyte migration and the distribution of ROS signaling. Previous studies have demonstrated that the presence of an osmotic gradient promotes keratinocyte migration via cell swelling[54]. Under control conditions, zebrafish are maintained in hypotonic water. Removing this osmotic gradient by wounding larvae in the presence of solution that is isotonic to the interstitial fluid has previously been shown to inhibit keratinocyte migration following mechanical injury and impair wound healing[49,54]. We found that wounding in the presence of an isotonic solution prevented the rapid movement of keratinocytes in response to a burn. Within the first hour following burn injury, keratinocyte average speed was reduced from 0.059 μm/s in control medium to 0.003 μm/s in isotonic medium (**Fig. 5A-C; Supplemental Movie 4**). Immediately following burn injury, the level of H_2O_2 was the same between the treatment groups, indicating that cells wounded in the presence of isotonic solution maintain their normal ability

to generate ROS (**Fig. 5F, G**)[55]. Examining ROS production during the first hour post-burn revealed that control larvae had increased ROS throughout the fin tissue compared to isotonic-treated larvae, while both conditions had comparable levels of ROS at the wound (**Fig. 5D, E**). At 6 hours post burn, H_2O_2 production was no longer localized to the wound edge in control burned larvae and had increased throughout the tailfin. By contrast, H_2O_2 remained restricted to the wound edge in larvae burned in the presence of isotonic solution, displaying a similar localized pattern to that observed after mechanical injury (**Fig. 5F**)[53,57]. Quantification revealed that H_2O_2 level at the wound edge was similar between control and isotonic treated larvae 6 hpb. However, the level of H_2O_2 was approximately 6-fold lower in the fin epithelial tissue adjacent to the burn wound with isotonic treatment (**Fig. 5F, H**). These findings suggest that robust keratinocyte movement induced by burn injury generates an oxidative environment at the tissue-scale.

Isotonic medium is sufficient to rescue sensory neuron regeneration and function after burn

To determine if isotonic treatment is sufficient to rescue sensory neuron function after burn, we assessed sensory neuron damage after burning in isotonic solution. Immediately following injury, larvae burned in isotonic solution displayed axonal damage similar to larvae injured in control medium (**Fig. 6A**). However, 6 hpw, axonal damage in isotonic treated larvae was reduced and remained restricted to the site of injury, similar to the spatially restricted H_2O_2 signal induced by isotonic treatment (**Fig. 6B**). Accordingly, larvae burned in isotonic medium had significantly greater axon density 24 hpw, and more than 85% of isotonic treated larvae had restored sensory function by 24 hpb (**Fig. 6C-E**). To determine if the benefit of isotonic solution was due to its ionic composition, we tested the effects of an isotonic solution of the sugar D-Sorbitol. We also found that an isotonic solution with D-Sorbitol limited basal keratinocyte migration and restored axon density and sensory function 24 hpw, suggesting that the benefit of isotonic solution is independent of effects on electrical cues (**Fig. S2B-D**).

To determine if early keratinocyte migration contributes to the impact of isotonic solution on sensory neuron function at later time points, we treated with isotonic solution starting 1 hour following burn injury (**Fig. 6F**). When isotonic medium was added 1 hpw, after keratinocyte migration was complete, there was no rescue

of ROS production in either the wound area or the fin 6 hpb (**Fig. 6 G, H**). Additionally, there was no improvement in sensory axon density or function 24 hpw, supporting the idea that early wound events during the first hour are critical for their effects on later sensory neuron function (**Fig. 6I-K**). Collectively, these findings suggest that early keratinocyte movement after burn coordinates spatial redox signaling and efficient sensory axon regeneration.

Discussion

Tissue repair requires the coordination of signaling across spatial and temporal scales. Our prior work has shown that early ROS signaling immediately after mechanical damage is necessary for longer term tissue repair[58]. Wound-induced ROS production is also required for leukocyte recruitment, ECM remodeling, and sensory neuron regeneration in response to tissue injury[20,29,59,60]. While the requirement of ROS production following tissue injury is clear, we lack an understanding of how early redox signaling is coordinated temporally and spatially to mediate long-term tissue repair. We recently reported that burn injury induces a distinct repair response with impaired collagen remodeling and delayed healing[27,29]. In light of the known defect in sensory function after burn injuries in humans, we sought to determine how the early epithelial response modulates sensory neuron recovery. Our findings suggest that early damage-induced keratinocyte movement plays a role in the spatial patterning of ROS production in the wound microenvironment, and impacts the ability of sensory neurons to regenerate.

Collective keratinocyte migration is conserved across species and is required to mediate wound closure after tissue injury[61,62]. While collective cell migration has been observed in larval zebrafish previously[63,64], its contribution to tissue repair remains unclear. In comparison to the organized movement associated with keratinocyte response to mechanical injury, our observations here identify excessive keratinocyte migration as a defining feature of the response to burn injury. Basal keratinocyte migration following burn injury appeared to lack a stereotypical leader-follower dynamic, with cells instead moving independently of one another but as a collective group. This observation suggests that collective keratinocyte migration is a feature of tissue repair in larval zebrafish regardless of the mode of injury and that its regulation is required for the success of long-term

healing. Indeed, we provide evidence that early migration and formation of lamellipodia in basal keratinocytes requires Arp2/3 signaling, and that this aberrant migration regulates the temporal and spatial distribution of early redox signaling in the wound tissue. However, Arp2/3 inhibition did not lead to sustained control of keratinocyte migration and production of ROS eventually increased throughout the tail fin. Accordingly, sensory function was not significantly improved at 24 hours post wound.

To further modulate keratinocyte movement we took advantage of osmotic regulation that is known to affect keratinocyte migration after wounding by tail fin transection. Cell swelling is thought to induce migration by promoting branched actin polymerization and lamellipodia formation[66–68], potentially through the activity of mechanically-activated ion channels. Previous groups have shown that osmotic differences trigger both ATP release and lamellipodia formation in basal keratinocytes, which promote keratinocyte migration[54,69]. Our results also show that osmotic modulation is critical for basal keratinocyte motility in response to burn injury. Interestingly, limiting keratinocyte motility by isotonic treatment is detrimental to tissue repair following mechanical injury[54], but isotonic treatment both rescues epithelial morphology and reduces axon damage following thermal injury. This suggests that there is an optimal amount of keratinocyte movement needed for efficient repair and long-term regeneration.

A conceptual challenge in wound repair has been understanding how early wound-induced events are linked to long-term repair[70]. ROS signaling provides a framework to understand this link due to its requirement for both early wound contraction and long-term regeneration. In zebrafish, the reactive oxygen species H_2O_2 is generated along a tissue-scale gradient with the highest levels at the wound edge[60]. While this spatial gradient undoubtedly directs cell function based on the position along the gradient, uncontrolled ROS production is damaging to tissues. Therefore, a mechanism must exist to control ROS such that it remains relatively localized to the site of damage and is controlled temporally and spatially. In addition to their early role in wound resealing, keratinocyte redox signaling is critical for long-term repair. Cell swelling induces $cPLA_2$-dependent 5-oxoETE production and immune cell recruitment[71]. This suggests the signals that control keratinocyte motility may simultaneously modify long-term keratinocyte signaling.

Our findings suggest that cell migration can modulate tissue scale signaling following injury. Importantly, isotonic treatment blocks keratinocyte movement and restores localized ROS signaling at the wound edge. The dependence on migration was supported both by the effects of Arp2/3 inhibition on early ROS signaling, and by the finding that isotonic treatment started after migration was complete (1 hour after injury) did not rescue tissue scale ROS. This suggests that early keratinocyte migration patterns the tissue scale ROS distribution. The finding that isotonic treatment at the time of injury was sufficient to rescue sensory function but treatment after 1 hour did not rescue axon regeneration highlights the important of this early motile response for setting up the longer term repair after damage.

The benefit of a system in which keratinocyte motility controls downstream signaling is two-fold. First, it enables signaling to be scaled to the size of injury. If more cells migrate due to a larger injury, then production of ROS will likewise increase. Second, this system provides a mechanism to control the spatial localization of signaling. Keratinocyte migration requires transiently detaching from neighboring cells. Thus, the act of migrating induces a physical change in the tissue that demarcates the wound region from healthy tissue. It is known that production of ROS promotes keratinocyte motility, and that adhesion is linked to cellular redox state[13,72]. Given these observations, it seems plausible that ROS production in wounded tissue is linked to the biomechanical state of keratinocytes – with low ROS in static, adhered cells, and high ROS in loosely adhered or migrating cells. A conceptual framework such as this would explain excessive ROS production in burn wounded tissue. Early keratinocyte dynamics in burned tissue are associated with normal wound edge ROS production. However, lack of a migratory stop signal may result in excessive keratinocyte migration and subsequent epithelial damage associated with keratinocytes detaching from the basal lamina. Therefore, failure to restore epithelial homeostasis due to unabated keratinocyte movement may allow for ROS production to continue over time and spread further away from the wound site. Future studies will be aimed at identifying the molecular link between cell migration and tissue scale signaling during tissue repair.

In summary, we have identified early wound-induced keratinocyte migration as a mechanism that controls spatial patterning of long-term wound signaling. These findings highlight the ability of keratinocytes within the wound microenvironment to integrate early signaling and migratory functions that mediate initial

wound closure and subsequently regulate spatial tissue signaling necessary for efficient repair of sensory neuron function. Further, our results not only highlight the utility of larval zebrafish for revealing new insights of the tissue response to injury *in vivo*, but also demonstrate the potential for these findings to inform new treatment strategies for wound healing more broadly.

Materials & Methods

Ethics

This study was carried out in accordance with the recommendations from the Guide for the Care and Use of Laboratory Animals from the National Institutes of Health. All zebrafish protocols in this study were approved by the University of Wisconsin-Madison Research Animals Resource Center (Protocol M005405-R02).

Zebrafish maintenance and handling

Adult zebrafish and embryos were maintained as described previously[27,73]. For all experiments, 3 days post-fertilization (dpf) larvae were anesthetized in E3 medium containing 0.2 mg/mL Tricaine (ethyl 3-aminobenzoate; Sigma-Aldrich) and maintained at 28.5 °C. All transgenic lines including *Tg(Ngn1:GFP-Caax)*[31], *Tg(Krt4:LifeAct-mRuby)*[74], *Tg(Krt4:UtrCH-GFP)*, *Tg(Krt4:TdTomato)*, *TgBac(Lamc1:Lamc1-sfGFP)*[64], *Tg(ElavI3:GCaMP5)*[75], *Tg(Krtt1c19e:LifeAct-mRuby)*, and *Tg(Krtt1c19e:acGFP)* were maintained on the AB background strain. To screen larvae for fluorescence, a Zeiss Zoomscope EMS3/SyCoP3 with a Plan-NeoFluar Z objective was used.

Generation of *Tg(Krtt1c19e:LifeAct-mRuby)* transgenic line

The *Krtt1c19e* promoter[47] flanked by Age1 and NotI was isolated and cloned into an expression vector containing Lifeact-mRuby and Tol2 elements for genomic integration. 3 nL of solution made of 50 ng DNA and 25 ng Tol2 transposase mRNA were injected into the yolk of one-cell stage embryos. F_0 larvae were raised to adulthood and crossed to adult AB zebrafish. F_2 larvae were screened for mRuby expression and grown to

generate stable lines. *Tg(Ngn1:GFP-Caax)* larvae transiently expressing *Krtt1c19e:Lifeact-m*Ruby were used for simultaneous imaging of neuron-keratinocyte interactions, and larvae transiently expressing *Krtt1c19e:Lifeact-mRuby* were used to acquire timelapses of basal keratinocyte migration in the CK666 treatment condition.

Caudal fin transection and burn injury

All injuries were applied to fish anesthetized in 1x Tricaine with E3. Transection of the caudal fin was performed on anesthetized larvae in a 60 mm tissue culture-treated dish containing 1x Tricaine with E3. Larvae were cut perpendicular to the caudal notochord boundary using a surgical blade (Feather No. 10, VWR). Burn injury was performed on anesthetized larvae in a 60 mm tissue culture-treated dish containing 1x Tricaine with E3. A fine tip cautery pen (Geiger Medical Technologies) was used to burn the caudal fin until the wounded region bordered but did not touch the posterior notochord boundary. After injury, larvae were kept in 60 mm dishes and maintained at 28.5 C until imaging. For two-wound experiments, larvae were either transected or burned as described above with the exception that injury was applied halfway to the notochord boundary to leave adequate room for secondary transection. Secondary transection, after either 5 minutes or 6 hours, was performed as described above.

Drug treatment

For all treatments, larvae were incubated in the indicated drug solution for at least 15-30 minutes. Each drug solution was made containing 1x Tricaine with E3 to keep fish anesthetized. Unless indicated otherwise, larvae were in the presence of treatment for the duration of all experiments. All treatments did not obviously impair larval development or health. To elicit sensory axon damage in the absence of a wound, larvae were treated with 1.5% sodium azide (Fisher Scientific). Isotonic medium was prepared by supplementing 1x Tricaine with E3 with either NaCl (Fisher Scientific) or D-Sorbitol (Sigma-Aldrich) to a final concentration of 135 mM. Isotonic medium does not noticeably impair embryonic development or health of the larvae on the time scale used

here[53,54]. For experiments using CK666 (Sigma), larvae were incubated in 100 µM Ck666 for one hour before wounding.

Live and time-lapse imaging

Larvae were imaged using a spinning disc microscope (CSU-X, Yokogawa) with a confocal scanhead on a Zeiss Observer Z.1 inverted microscope, Plan-Apochromat NA 0.8/20X objective, and a Photometrics Evolve EMCCD camera. All images were acquired using ZEN 2.6 software. For time lapse imaging, larvae were mounted in a zWEDGI restraining device[76] with the head covered in 2% low-melting point agarose (Sigma-Aldrich). For single time point imaging, anesthetized larvae were mounted in 2% low-melting point agarose on a 35 mm glass-bottom depression dish (CellVis). In all cases, larvae were imaged in E3 medium supplemented with Tricaine as described above.

Quantification of axon density and sensory function

Axon density was measured by generating maximum intensity z-projected confocal images of the caudal fin using FIJI[77]. For every experiment, the caudal fin area posterior to the notochord was outlined using the Polygon tool and measured to obtain a total surface area ROI. Axons inside the outlined area were manually thresholded so all axons posterior to the notochord were labeled and no saturated pixels were present. Density was measured by dividing the area of detected axons by the area of the ROI. In each case, density values of the experimental sample were normalized to the indicated control - either unwounded or control treated fins.

Sensory neuron function was determined using a behavioral touch assay[34]. 3-day post-fertilization larvae were wounded as described above. At the indicated time post-wound, larvae were briefly anesthetized for mounting into the zWEDGI restraining device, with only the head mounted in 2% low-melting point agarose. Fresh E3 was added and larvae were allowed to rest for one hour. To assess sensory function, the wounded region of caudal fin was touched with the tip of an eyelash brush (No. 1 Superfine Eyelash, Ted Pella) and the presence or absence of a twitch reflex was recorded.

Visualization of sensory axon and tissue damage

To visualize damage to sensory axons, *Tg(ElavI3:GCaMP5)* larvae were used. Identical microscope settings (20x objective, 10% laser, 100 ms exposure, 2 µm step size) were used for all experiments to acquire images and movies. Representative images are maximum intensity z-projections of the caudal fin generated using FIJI. FM 1-43 dye (Life Technologies) was used to visualize tissue damage following transection and burn injury. For these experiments, larvae were incubated in 1 mg/ml FM 1-43 for 15 minutes prior to injury and through time at which they were imaged. Larvae were maintained at 28.5 C until imaging at the indicated time post-injury.

Quantification of hydrogen peroxide level

Hydrogen peroxide was quantified using pentafluorobenzenesulfonyl fluorescein (Pfbsf, Santa Cruz)[78]. Larvae were incubated in 1 µM Pfbsf for 15 minutes prior to injury and maintained in dye solution for the duration of each experiment. Identical microscope settings (10x objective, 1% laser, 50 ms exposure, 3.7 µm step size) were used for all experiments to acquire images and movies. Pfbsf intensity was calculated by generating sum projections and measuring mean gray value of the fin and wound zone in FIJI. Wound zone Pfbsf quantifications were taken by measuring mean gray value of the area posterior to the notochord. For measurements of the fin, mean gray value of the trunk area 200 µm anterior to the tip of the notochord and excluding pigmented skin within the region was measured. Background signal was subtracted for each measurement.

Cell tracking

Basal keratinocyte tracking following tissue injury was performed using *Tg(Krtt1c19e:acGFP)* larvae. Cell tracking was performed using the Spots module in Imaris version 9.8.2 (Bitplane, Zurich, Switzerland). For each larva, 3 representative cells were identified and manual tracking was performed, with the average of these cells being used to generate a single value for further analysis. To control for drift of the entire fin during imaging, non-moving pigment was manually tracked by Brightfield and track length was subtracted from basal

keratinocyte movement. In all cases, larvae were imaged for 1 hour following injury at an interval of 30 seconds.

Morpholino injection

Ngn1 morpholino with the sequence 5'-ACG ATC TCC ATT GTT GAT AAC CTG G-3'[79] was used to prevent sensory neuron formation in Elavl3-GCaMP5 larvae to confirm damage signals were constrained only to axons. 5 ng of Ngn1 morpholino was injected into the yolk of one- to two-cell stage zebrafish embryos. Larvae were incubated at 28.5 C until used for experiments at 3 days post-fertilization. Before use in experiments, larvae were screened by the sensory function assay described above to ensure that sensory neurons were depleted.

Image processing

Images were processed and analyzed using FIJI and Imaris version 9.8.2 as indicated. Supplemental movies were generated in FIJI and edited using Adobe Premiere Pro (Adobe). In Adobe Premiere Pro, pseudocoloring of individual keratinocytes was done using the Color Effects module with manual tracking.

Statistical analysis

Each experimental condition consists of at least three independent biological replicates, defined as three clutches of larvae spawned on three different days. Cell-tracking experiments were analyzed using non-parametric methods (Wilcoxon rank-sum test). Quantification of axon density was analyzed using linear mixed-effect models in which biological replicate was treated as a random effect and experimental conditions (e.g., wound, time, or chemical treatment) treated as fixed factors. Experiments measuring fluorescence intensity (Pfbsf intensity) were analyzed in the same manner, except the response (fluorescence) was log-transformed prior to analysis. Means computed on the log scale estimate the median response when back transformed to original units. At the same time, differences between means (of log-transformed data) become ratios of medians after back transformation to the original scale[80]. Experiments involving the proportion of fish that responded to touch were analyzed using a general linear model that included replicate and experimental condition as fixed

effects; standard errors used for estimation and testing were adjusted to correct for heteroscedasticity in the proportions[81]. Graphing was performed using GraphPad Prism 9 (GraphPad Software, Inc, San Diego, CA). Sample size is reported for specific experiments in the figure legends.

Acknowledgements

We would like to thank Dr. Mary Halloran (University of Wisconsin-Madison) for the gift of the *Tg(Ngn1-GFP-Caax)* fish line, Dr. Jan Huisken (University of Göttingen) for the *Tg(Elavl3-GCaMP5)* fish line, Dr. Alvaro Sagasti (University of California Los Angeles) for the *Tg(Krtt1c19e:acGFP)* fish line, and Dr. Holger Knaut (New York University) for the *TgBac(LamC1:LamC1-sfGFP)* fish line. We would like to thank Taylor Schoen and Veronika Miskolci for their critical reading of the manuscript, and the members of the Huttenlocher lab for their thoughtful input throughout this project. The authors acknowledge K99 GM147303 to Adam Horn and R35 GM118027 to Anna Huttenlocher.

Author Contributions

A. Fister, A. Horn, and A. Huttenlocher designed and planned the experimental approach. A. Fister and A. Horn performed all the experiments. M. Lasarev performed all statistical analysis. A. Fister, A. Horn, and A. Huttenlocher wrote the paper.

Declaration of Interests

The authors declare no competing financial interests.

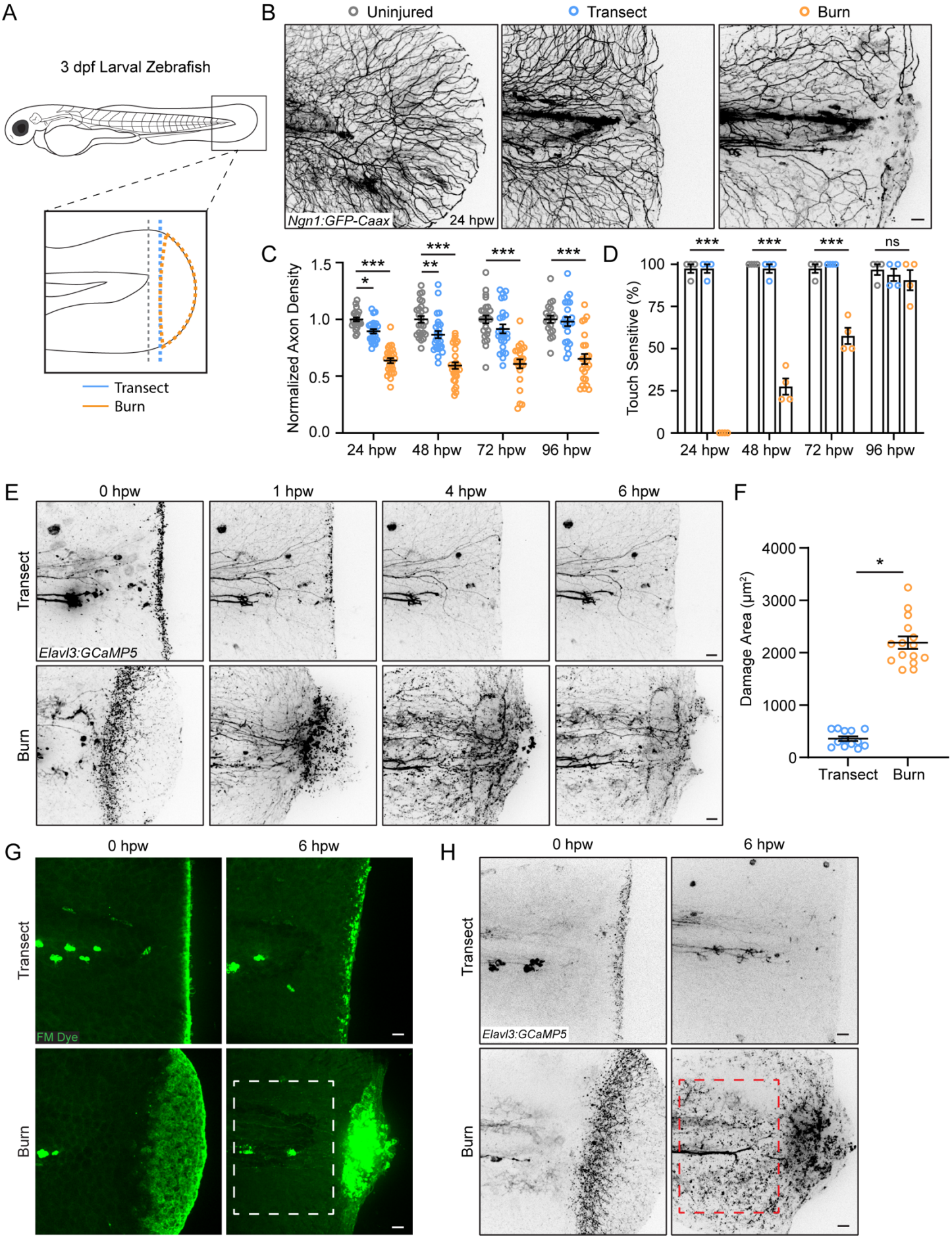
A
3 dpf Larval Zebrafish
Transect
Burn
B
Uninjured
Transect
Burn
Ngn1:GFP-Caax
24 hpw
C
Normalized Axon Density
1.5
1.0
0.5
0.0
***
*
***
**
***
***
24 hpw
48 hpw
72 hpw
96 hpw
D
Touch Sensitive (%)
100
75
50
25
0
***
***
***
ns
24 hpw
48 hpw
72 hpw
96 hpw
E
0 hpw
1 hpw
4 hpw
6 hpw
Transect
Burn
Elavl3:GCaMP5
F
Damage Area (μm²)
4000
3000
2000
1000
0
*
Transect
Burn
G
0 hpw
6 hpw
Transect
Burn
FM Dye
H
0 hpw
6 hpw
Transect
Burn
Elavl3:GCaMP5

Figure 1: Peripheral sensory neurons have impaired regeneration after burn injury. (A) Schematic of larval zebrafish injury. Gray dashed line denotes area used to measured axon density to the right of the notochord. (B) Confocal max-projected images of sensory neurons in uninjured, transected, and burned *Tg(Ngn1:GFP-Caax)* caudal fins 24 hpw. (C) Quantification of axon density for uninjured, transected, and burned larvae in the wound area 24-96 hpw. N>20 larvae per condition from 4 replicates. (D) Quantification of sensory perception for uninjured, transected, and burned larvae 24-96 hpw. N>32 larvae per condition from 4 replicates. (E) Confocal time series images of axonal damage, indicated by calcium-positive punctae (black dots), in *Tg(Elavl3:GCaMP5)* larvae following either transection or burn injury. (F) Quantification of axon damage area in transected and burned larvae 6 hpw. N>12 larvae per condition from 2 replicates. (G) Images of larvae either transected or burned in the presence of FM 1-43 dye. White dashed box denotes area of uninjured tissue in which axonal damage appears in H. (H) Images show axonal damage following transection or burn injury. Red dashed box corresponds to the tissue region highlighted in G. In all cases, scale bars=20 µm. *p<0.05, **p<0.01, ***p<0.001, ns=not significant.

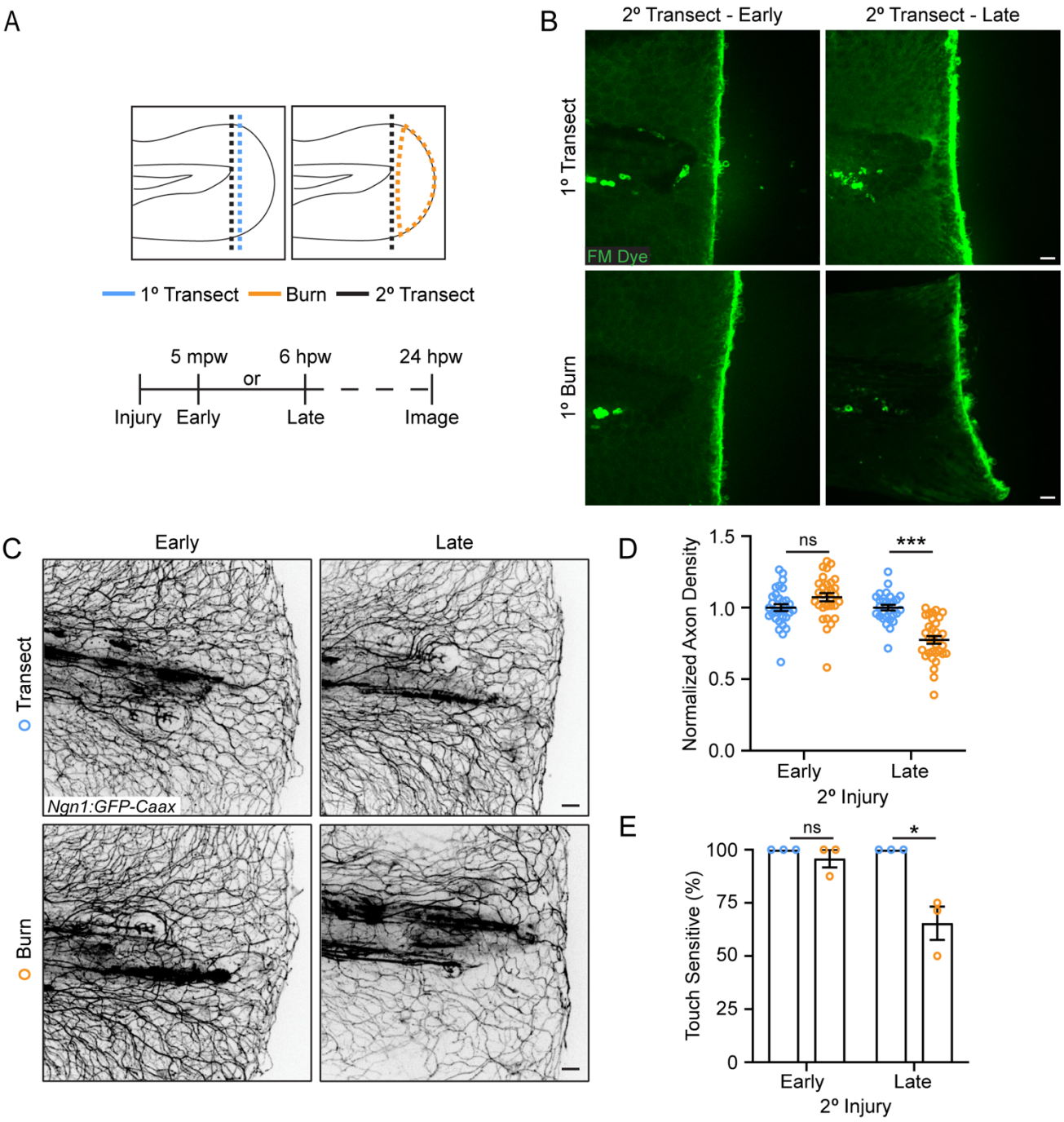

Figure 2: The burn wound microenvironment contributes to impaired sensory neuron regeneration. (A) Schematic of two-wound experiment design. (B) Confocal max-projected images of FM dye staining following secondary transection in the two-wound experiment at 5 mpw and 6 hpw. (C) Images of sensory neurons in larvae subjected to an initial transection or burn injury followed by subsequent transection either early (5 mpw) or late (6 hpw). (D) Quantification of axon density in wounded tissue 24 hpw from larvae wounded as in B. N>28 larvae per condition from 3 replicates. (E) Quantification of sensory perception in

wounded tissue 24 hpw from larvae wounded as in B. N=24 larvae each from 3 replicates. In all cases, scale bars=20 µm. *$p<0.05$, ***$p<0.001$, ns=not significant.

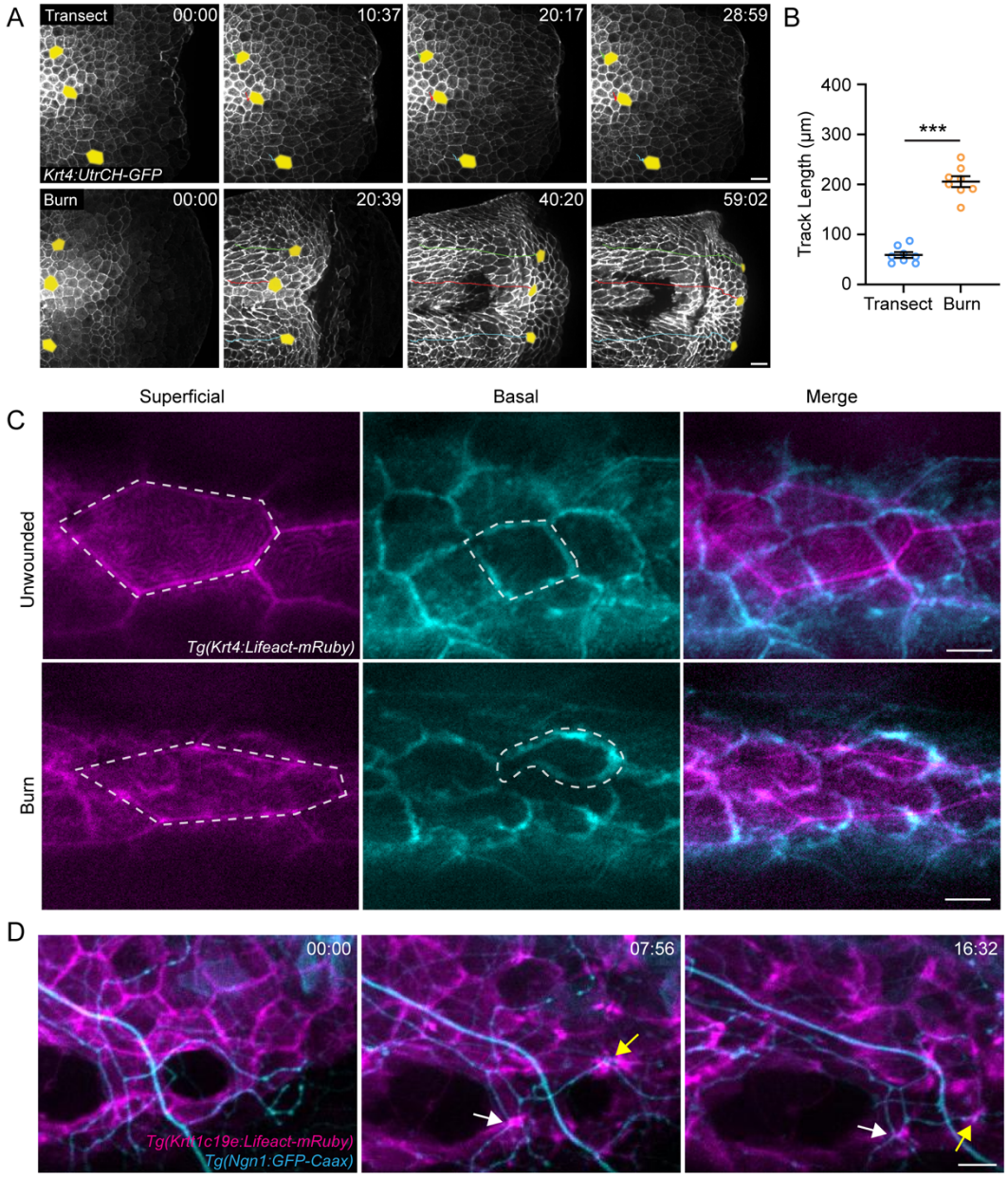

Figure 3: Burn injury induces coordinated keratinocyte and sensory neuron movement. (A) Confocal max-projected time-series images of *Tg(Krt4:UtrCH-GFP)* larvae after either transection or burn injury. Yellow pseudocolored cells and colored tracks highlight keratinocyte displacement. Scale bar=20 µm. (B) Quantification of keratinocyte movement distance over 1 hpw. N= 8 larvae each collected from 3 replicates. (C) Confocal max-projected images of superficial and basal keratinocytes in *Tg(Krt4:Lifeact-mRuby)* labeled larvae. Left, superficial keratinocytes. Middle, basal keratinocytes. Right, Merge. Dashed lines outline one individual keratinocyte. Scale bar=10 µm. (D) Confocal max-projected time-series images of sensory neurons

and basal keratinocytes in dual-labeled *Tg(Krt4:Lifeact-mRuby); Tg(Ngn1:GFP-Caax)* larvae unwounded or after burn. Arrows highlight coincident movement between keratinocytes and associated sensory neurons. Unless otherwise stated, scale bar=20 µm. ***$p<0.001$.

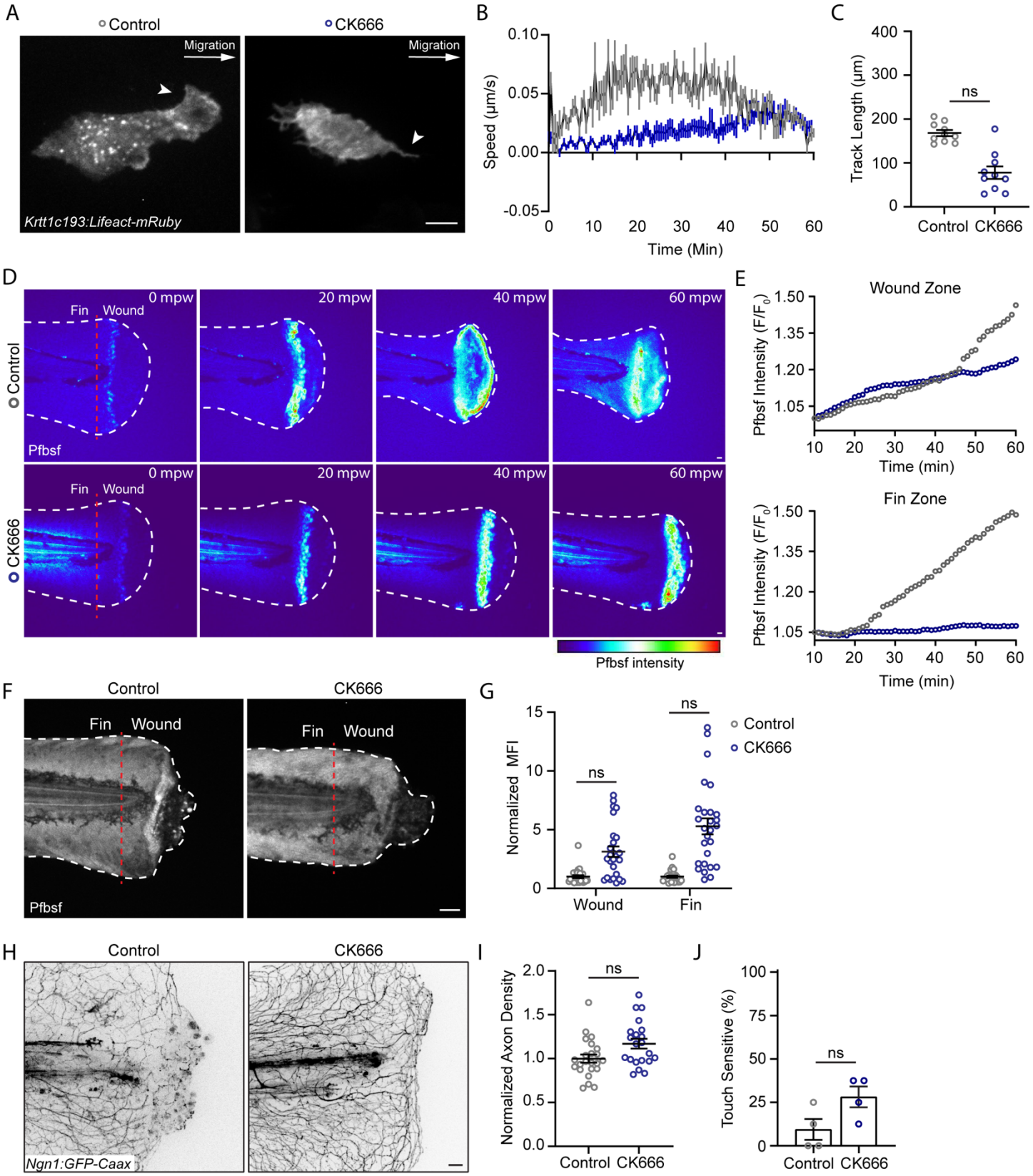
A
Control
CK666
Migration
Migration
Krtt1c193:Lifeact-mRuby
B
Speed (µm/s)
Time (Min)
C
Track Length (µm)
ns
Control
CK666
D
0 mpw
20 mpw
40 mpw
60 mpw
Fin
Wound
Control
CK666
Pfbsf
Pfbsf intensity
E
Wound Zone
Fin Zone
Pfbsf Intensity (F/F0)
Time (min)
F
Control
CK666
Fin
Wound
Pfbsf
G
Normalized MFI
ns
Wound
Fin
Control
CK666
H
Control
CK666
Ngn1:GFP-Caax
I
Normalized Axon Density
ns
Control
CK666
J
Touch Sensitive (%)
ns
Control
CK666

Fig. 4: Inhibition of keratinocyte migration with the Arp 2/3 inhibitor CK666 improves, but does not fully rescue, burn outcomes. (A) Confocal max-projected images of control or CK666-treated transiently injected *Tg(Krtt1c19e:Lifeact-mRuby)* larvae. Arrows point to lamellipodia in the control larva, and lack of lamellipodia in the CK666-treated larva. Scale bar=10 µm. (B) Plot of keratinocyte speed over 1 hpw as treated in A. N=10 larvae each collected from 3 replicates. (C) Plot of keratinocyte distance moved over 1 hpw as treated in A . N=10 larvae each collected form 3 replicates. (D) Confocal sum-projected time-series images of hydrogen peroxide level (Pfbsf intensity) over 1 hpw in the indicated treatment. (E) Quantification of Pfbsf intensity in the wound or fin area after burn injury as treated in D over 1 hpw. (F) Confocal sum-projected images of mean Pfbsf fluorescence intensity in larvae 6 hpw with the indicated treatment. Dashed red line denotes the boundary between the wound area and distal fin tissue. White dashed line outlines the fin. (G) Quantification of mean Pfbsf fluorescence intensity (Mean Fluorescence Intensity, MFI) 6 hpw in the indicated region of the fin normalized to the control condition. N>26 larvae per condition from 3 replicates. (H) Confocal max-projected images of sensory neurons 24 hpw in larvae wounded in control medium or CK666. (I) Quantification of axon density 24 hpw in larvae treated as in J. N>22 larvae per condition from 4 replicates. (J) Quantification of sensory perception 24 hpw in larvae treated as in J. N=32 larvae per condition from 4 replicates. Unless otherwise specified, scale bars=20 µm. ns=not significant.

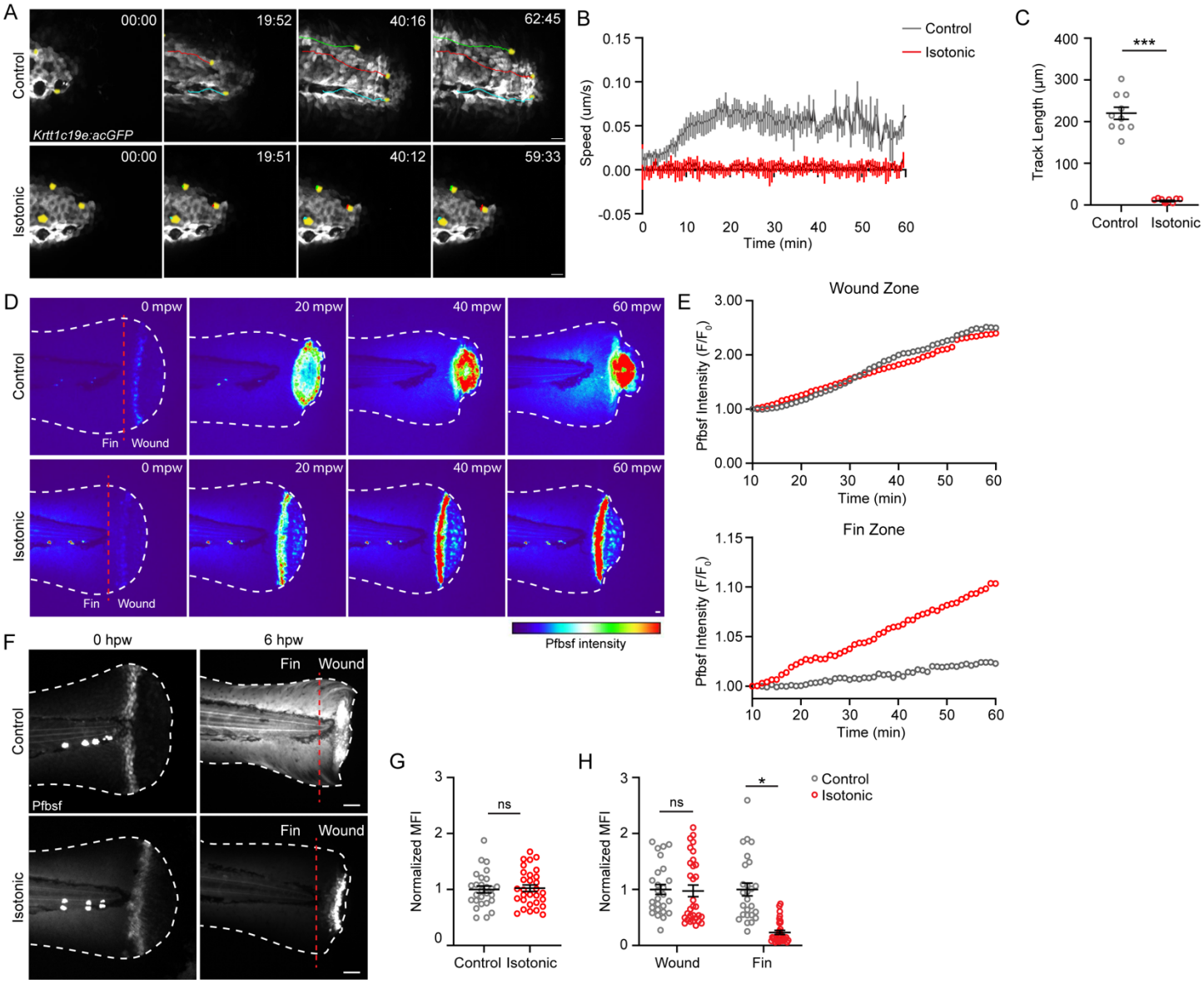

Figure 5: Dysregulated keratinocyte migration causes sustained epidermal damage and loss of localized reactive oxygen species signaling. (A) Confocal time-series images of basal keratinocyte movement in *Tg(Krtt1c19e:acGFP)* larvae over 1 hpw after burn injury in the indicated treatment. (B) Plot of basal keratinocyte average speed over 1 hpw treated as in A. N=10 larvae per condition collected from 3 replicates. (C) Distance of keratinocyte movement over 1 hpw treated as in A. N=10 larvae per condition collected from 3 replicates. (D) Confocal sum-projected time-series images of hydrogen peroxide level (Pfbsf intensity) over 1 hpw as treated in A. (E) Quantification of Pfbsf intensity in the wound or fin area after burn injury as treated in D over 1 hpw. N=1 representative larva per condition. (F) Confocal sum-projected images of Pfbsf intensity in the fin and wound zone either 0 or 6 hours following burn injury. Dashed red line denotes the boundary between

the wound area and distal fin tissue. Scale bar=50 µm. (G) Quantification of mean Pfbsf fluorescence intensity (MFI) immediately (0 hpw) after burn injury normalized to the control condition. N>27 larvae per condition from 3 replicates. (H) Quantification of mean Pfbsf fluorescence intensity 6 hpw in the indicated region of the fin normalized to the control condition. N>26 larvae per condition from 3 replicates. Unless otherwise indicated, scale bars=20 µM. *$p<0.05$, ***$p<0.001$, ns=not significant.

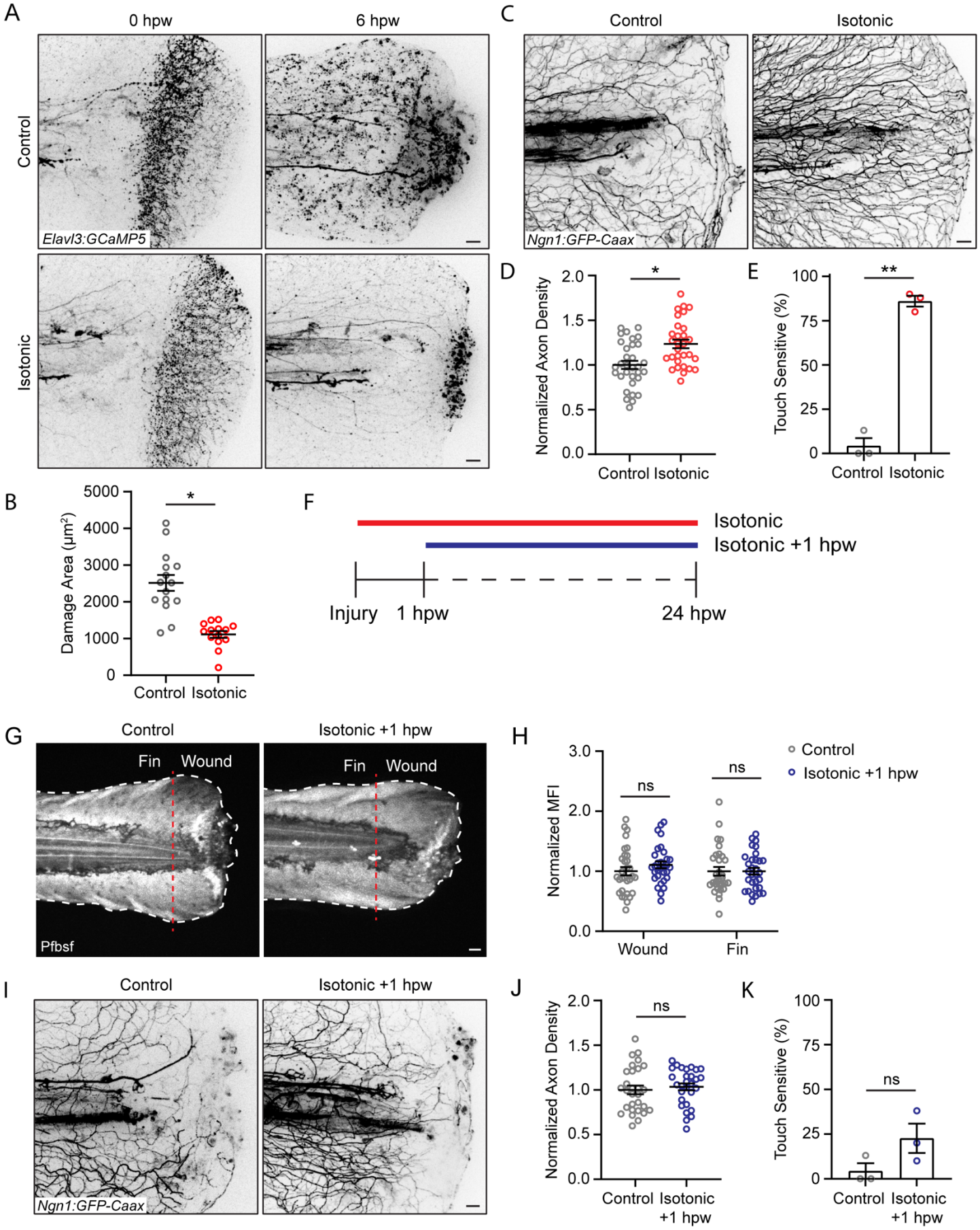
A
0 hpw
6 hpw
Control
Isotonic
Elavl3:GCaMP5
C
Control
Isotonic
Ngn1:GFP-Caax
D
Normalized Axon Density
2.0
1.5
1.0
0.5
0.0
*
Control Isotonic
E
Touch Sensitive (%)
100
75
50
25
0
**
Control Isotonic
B
Damage Area (μm²)
5000
4000
3000
2000
1000
0
*
Control Isotonic
F
Isotonic
Isotonic +1 hpw
Injury
1 hpw
24 hpw
G
Control
Isotonic +1 hpw
Fin
Wound
Pfbsf
H
Normalized MFI
3.0
2.0
1.0
0.0
ns
ns
Wound
Fin
Control
Isotonic +1 hpw
I
Control
Isotonic +1 hpw
Ngn1:GFP-Caax
J
Normalized Axon Density
2.0
1.5
1.0
0.5
0.0
ns
Control
Isotonic +1 hpw
K
Touch Sensitive (%)
100
75
50
25
0
ns
Control
Isotonic +1 hpw

Figure 6: Excessive keratinocyte movement immediately after burn injury impairs sensory neuron regeneration. (A) Confocal max-projected images of axon damage in control or isotonic treated *Tg(Elavl3:GCaMP5)* larvae 0 or 6 hpw. (B) Quantification of axon damage in control and isotonic treated burned fins at 6 hpw as treated in A. N=16 larvae per condition from 3 replicates. (C) Confocal max-projected images of sensory neurons in larvae 24 hpw as treated in A. (D) Quantification of axon density 24 hpw in larvae treated as depicted in C. N>30 larvae per condition from 3 replicates. (E) Quantification of sensory perception 24 hpw in larvae treated as in C. N=24 larvae each from 3 replicates. (F) Schematic illustrating the different isotonic treatment paradigms. (G) Confocal sum-projected images of pfbsf intensity in control and isotonic +1 hpw treated burned larvae. Dashed red line denotes the boundary between the wound area and distal fin tissue. White dashed line denotes the fin. (H) Quantification of mean Pfbsf fluorescence intensity (MFI) 6 hpw in the indicated region of the finnormalized to the control condition. N=31 larvae per condition from 3 replicates. (I) Confocal max-projected images of sensory neurons 24 hpw in burned control or isotonic treated larvae starting 1 hpw. (J) Quantification of axon density 24 hpw in larvae treated as in I. N=29 larvae per condition from 3 replicates. (K) Quantification of sensory perception 24 hpw in larvae treated as in I. N=24 larvae per condition from 3 replicates. Unless otherwise indicated, scale bars=20 μm. *$p<0.05$, **$p<0.01$, ns=not significant.

References

1. DiAntonio, A. (2019). Axon degeneration: mechanistic insights lead to therapeutic opportunities for the prevention and treatment of peripheral neuropathy. Pain *160*, S17–S22. 10.1097/J.PAIN.0000000000001528.
2. Li, Y., Pazyra-Murphy, M.F., Avizonis, D., de Sá Tavares Russo, M., Tang, S., Chen, C.Y., Hsueh, Y.P., Bergholz, J.S., Jiang, T., Zhao, J.J., et al. (2022). Sarm1 activation produces cADPR to increase intra-axonal Ca++ and promote axon degeneration in PIPN. J Cell Biol *221*. 10.1083/jcb.202106080.
3. Rabiller, L., Labit, E., Guissard, C., Gilardi, S., Guiard, B.P., Moulédous, L., Silva, M., Mithieux, G., Pénicaud, L., Lorsignol, A., et al. (2021). Pain sensing neurons promote tissue regeneration in adult mice. NPJ Regen Med *6*. 10.1038/s41536-021-00175-7.
4. Reyes, R., Haendel, M., Grant, D., Melancon, E., and Eisen, J.S. (2004). Slow Degeneration of Zebrafish Rohon-Beard Neurons during Programmed Cell Death. Developmental Dynamics *229*, 30–41. 10.1002/DVDY.10488.
5. Pope, H.M., and Voigt, M.M. (2014). Peripheral Glia Have a Pivotal Role in the Initial Response to Axon Degeneration of Peripheral Sensory Neurons in Zebrafish. PLoS One *9*, 103283. 10.1371/journal.pone.0103283.
6. Rasmussen, J.P., Sack, G.S., Martin, S.M., and Sagasti, A. (2015). Vertebrate Epidermal Cells Are Broad-Specificity Phagocytes That Clear Sensory Axon Debris. 10.1523/JNEUROSCI.3613-14.2015.
7. Mahar, M., and Cavalli, V. (2018). Intrinsic mechanisms of neuronal axon regeneration. Nat Rev Neurosci *19*, 323–337. 10.1038/S41583-018-0001-8.
8. Renthal, W., Tochitsky, I., Yang, L., Cheng, Y.C., Li, E., Kawaguchi, R., Geschwind, D.H., and Woolf, C.J. (2020). Transcriptional reprogramming of distinct peripheral sensory neuron subtypes after axonal injury. Neuron *108*, 128. 10.1016/J.NEURON.2020.07.026.
9. Liu, K., Tedeschi, A., Park, K.K., and He, Z. (2011). Neuronal Intrinsic Mechanisms of Axon Regeneration. https://doi.org/10.1146/annurev-neuro-061010-113723 *34*, 131–152. 10.1146/ANNUREV-NEURO-061010-113723.
10. Villegas, R., Martin, S.M., O, K.C., Carrillo, S.A., Sagasti, A., and Allende, M.L. (2012). Dynamics of degeneration and regeneration in developing zebrafish peripheral axons reveals a requirement for extrinsic cell types. Neural Dev *7*, 19. 10.1186/1749-8104-7-19.
11. Cheah, M., Fawcett, J.W., and Haenzi, B. (2017). Differential regenerative ability of sensory and motor neurons. Neurosci Lett *652*, 35–40. 10.1016/J.NEULET.2016.11.004.
12. Avraham, O., Feng, R., Ewan, E.E., Rustenhoven, J., Zhao, G., and Cavalli, V. (2021). Profiling sensory neuron microenvironment after peripheral and central axon injury reveals key pathways for neural repair. Elife *10*. 10.7554/ELIFE.68457.
13. Dunnill, C., Patton, T., Brennan, J., Barrett, J., Dryden, M., Cooke, J., Leaper, D., and Georgopoulos, N.T. (2015). Reactive oxygen species (ROS) and wound healing: the functional role of ROS and emerging ROS-modulating technologies for augmentation of the healing process. Int Wound J. 10.1111/iwj.12557.
14. Kuwabara, W.M.T., Zhang, L., Schuiki, I., Curi, R., Volchuk, A., and Alba-Loureiro, T.C. (2015). NADPH Oxidase-Dependent Production of Reactive Oxygen Species Induces Endoplasmatic Reticulum Stress in Neutrophil-Like HL60 Cells. PLoS One *10*. 10.1371/JOURNAL.PONE.0116410.
15. Sies, H., and Jones, D.P. (2020). Reactive oxygen species (ROS) as pleiotropic physiological signalling agents. Nature Reviews. 10.1038/s41580-020-0230-3.
16. Mittal, M., Siddiqui, M.R., Tran, K., Reddy, S.P., and Malik, A.B. COMPREHENSIVE INVITED REVIEW Reactive Oxygen Species in Inflammation and Tissue Injury. 10.1089/ars.2012.5149.

17. Linley, J.E., Ooi, L., Pettinger, L., Kirton, H., Boyle, J.P., Peers, C., and Gamper, N. (2012). Reactive oxygen species are second messengers of neurokinin signaling in peripheral sensory neurons. Proc Natl Acad Sci U S A *109*. 10.1073/PNAS.1201544109/-/DCSUPPLEMENTAL/PNAS.201201544SI.PDF.
18. Love, N.R., Chen, Y., Ishibashi, S., Kritsiligkou, P., Lea, R., Koh, Y., Gallop, J.L., Dorey, K., and Amaya, E. (2013). Amputation-induced reactive oxygen species (ROS) are required for successful Xenopus tadpole tail regeneration. Nat Cell Biol *15*, 222. 10.1038/NCB2659.
19. Montserrat, M., Romero, G., Mccathie, G., Jankun, P., Henry, &, and Roehl, H. (2018). Damage-induced reactive oxygen species enable zebrafish tail regeneration by repositioning of Hedgehog expressing cells. Nat Commun. 10.1038/s41467-018-06460-2.
20. Rieger, S., and Sagasti, A. (2011). Hydrogen Peroxide Promotes Injury-Induced Peripheral Sensory Axon Regeneration in the Zebrafish Skin. PLoS Biol *9*, 1000621. 10.1371/journal.pbio.1000621.
21. Cobb, C.A., and Cole, M.P. (2015). Oxidative and Nitrative Stress in Neurodegeneration HHS Public Access. Neurobiol Dis *84*, 4–21. 10.1016/j.nbd.2015.04.020.
22. Blais, M., Parenteau-bareil, R., Cadau, S., and Ois Berthod, F. Concise Review: Tissue-Engineered Skin and Nerve Regeneration in Burn Treatment. 10.5966/sctm.2012-0181.
23. Choinière, M., Melzack, R., and Papillon, J. (1991). Pain and paresthesia in patients with healed burns: An exploratory study. J Pain Symptom Manage *6*, 437–444. 10.1016/0885-3924(91)90043-4.
24. Tirado-Esteban, A., Seoane, J.L., Serracanta Domènech, J., Aguilera-Sáez, J., and Barret, J.P. (2020). Sensory alteration patterns in burned patients. Burns *46*, 1729–1736. 10.1016/J.BURNS.2019.08.005.
25. Pavoni, V., Gianesello, L., Paparella, L., Buoninsegni, L.T., and Barboni, E. (2010). Outcome predictors and quality of life of severe burn patients admitted to intensive care unit. Scand J Trauma Resusc Emerg Med *18*, 1–8. 10.1186/1757-7241-18-24/FIGURES/3.
26. Tsolakidis, S., Alharbi, Z., Rennekampff, H.O., Schmidhammer, M.R., Schmidhammer, R., and Rosenauer, R. (2022). “Out of Touch”—Recovering Sensibility after Burn Injury: A Review of the Literature. European Burn Journal *3*, 370–376. 10.3390/EBJ3020032/S1.
27. Miskolci, V., Squirrell, J., Rindy, J., Vincent, W., Sauer, J.D., Gibson, A., Eliceiri, K.W., and Huttenlocher, A. (2019). Distinct inflammatory and wound healing responses to complex caudal fin injuries of larval zebrafish. Elife *8*. 10.7554/ELIFE.45976.
28. LeBert, D.C., Squirrell, J.M., Rindy, J., Broadbridge, E., Lui, Y., Zakrzewska, A., Eliceiri, K.W., Meijer, A.H., and Huttenlocher, A. (2015). Matrix metalloproteinase 9 modulates collagen matrices and wound repair. Development (Cambridge) *142*, 2136–2146. 10.1242/DEV.121160/VIDEO-3.
29. LeBert, D., Squirrell, J.M., Freisinger, C., Rindy, J., Golenberg, N., Frecentese, G., Gibson, A., Eliceiri, K.W., and Huttenlocher, A. (2018). Damage-induced reactive oxygen species regulate vimentin and dynamic collagen-based projections to mediate wound repair. Elife. 10.7554/eLife.30703.001.
30. Andermann, P., Ungos, J., and Raible, D.W. (2002). Neurogenin1 Defines Zebrafish Cranial Sensory Ganglia Precursors. Dev Biol *251*, 45–58. 10.1006/DBIO.2002.0820.
31. Blader, P., Plessy, C., and Strähle, U. (2003). Multiple regulatory elements with spatially and temporally distinct activities control neurogenin1 expression in primary neurons of the zebrafish embryo. Mech Dev *120*, 211–218. 10.1016/S0925-4773(02)00413-6.
32. McGraw, H.F., Nechiporuk, A., and Raible, D.W. (2008). Zebrafish dorsal root ganglia neural precursor cells adopt a glial fate in the absence of neurogenin1. J Neurosci *28*, 12558–12569. 10.1523/JNEUROSCI.2079-08.2008.
33. Lisse, T.S., Brochu, E.A., and Rieger, S. (2015). Capturing Tissue Repair in Zebrafish Larvae with Time-lapse Brightfield Stereomicroscopy. J Vis Exp, 52654. 10.3791/52654.
34. Granato, M., van Eeden, F.J.M., Schach, U., Trowe, T., Brand, M., Furutani-Seiki, M., Haffter, P., Hammerschmidt, M., Heisenberg, C.P., Jiang, Y.J., et al. (1996). Genes controlling and mediating locomotion behavior of the zebrafish embryo and larva. Development *123*, 399–413. 10.1242/DEV.123.1.399.

35. Vargas, M.E., Yamagishi, Y., Tessier-Lavigne, M., and Sagasti, A. (2015). Live Imaging of Calcium Dynamics during Axon Degeneration Reveals Two Functionally Distinct Phases of Calcium Influx. Journal of Neuroscience *35*, 15026–15038. 10.1523/JNEUROSCI.2484-15.2015.
36. Khaitin, A. (2021). Calcium in Neuronal and Glial Response to Axotomy. Int J Mol Sci *22*. 10.3390/IJMS222413344.
37. Linsley, J.W., Shah, K., Castello, N., Chan, M., Haddad, D., Doric, Z., Wang, S., Leks, W., Mancini, J., Oza, V., et al. (2021). Genetically encoded cell-death indicators (GEDI) to detect an early irreversible commitment to neurodegeneration. Nat Commun, 1–14. 10.1038/s41467-021-25549-9.
38. Ziv, N.E., and Spira, M.E. (1993). Spatiotemporal Distribution of Ca2+ Following Axotomy and Throughout the Recovery Process of Cultured Aplysia Neurons. European Journal of Neuroscience *5*, 657–668. 10.1111/J.1460-9568.1993.TB00531.X.
39. Adalbert, R., Morreale, G., Paizs, À.M., Conforti, L., Walker, S.A., Roderick, H.L., Bootman, M.D., Siklo´s, L., Siklo´s, S., and Coleman, M.P. Intra-axonal calcium changes after axotomy in wild-type and slow wallerian degeration. 10.1016/j.neuroscience.2012.08.056.
40. Arrázola, M.S., Saquel, C., Catalán, R.J., Barrientos, S.A., Hernandez, D.E., Martínez, N.W., Catenaccio, A., and Court, F.A. (2019). Axonal Degeneration Is Mediated by Necroptosis Activation. Journal of Neuroscience *39*, 3832–3844. 10.1523/JNEUROSCI.0881-18.2019.
41. Defour, A., Sreetama, S.C., and Jaiswal, J.K. (2014). Imaging Cell Membrane Injury and Subcellular Processes Involved in Repair. J Vis Exp, 51106. 10.3791/51106.
42. Shannon, E.K., Stevens, A., Edrington, W., Zhao, Y., Jayasinghe, A.K., Page-McCaw, A., and Shane Hutson, M. Multiple Mechanisms Drive Calcium Signal Dynamics around Laser-Induced Epithelial Wounds. 10.1016/j.bpj.2017.07.022.
43. McDade, J.R., Naylor, M.T., and Michele, D.E. (2021). Sarcolemma wounding activates dynamin-dependent endocytosis in striated muscle. FEBS Journal *288*, 160–174. 10.1111/FEBS.15556.
44. Lauritzen Sønder, S., Laage Ebstrup, M., Dias, C., Sofie, A., Heitmann, B., and Nylandsted, J. (2022). Plasma Membrane Wounding and Repair Assays for Eukaryotic Cells. Bio Protoc *12*, 4437. 10.21769/BioProtoc.4437.
45. Rosa, J.B., Nassman, K.Y., and Sagasti, A. (2022). Sensory axons induce epithelial lipid microdomain remodeling and determine the distribution of junctions in the epidermis. Mol Biol Cell. 10.1091/MBC.E22-09-0396/ASSET/IMAGES/LARGE/MBC-34-AR5-G008.JPEG.
46. O'brien, G.S., Rieger, S., Wang, F., Smolen, G.A., Gonzalez, R.E., Buchanan, J., and Sagasti, A. (2012). Coordinate Development of Skin Cells and Cutaneous Sensory Axons in Zebrafish. J. Comp. Neurol *520*, 816–831. 10.1002/cne.22791.
47. Lee, R.T.H., Asharani, P. v., and Carney, T.J. (2014). Basal Keratinocytes Contribute to All Strata of the Adult Zebrafish Epidermis. PLoS One *9*, e84858. 10.1371/JOURNAL.PONE.0084858.
48. Park, S., Gonzalez, D.G., Guirao, B., Boucher, J.D., Cockburn, K., Marsh, E.D., Mesa, K.R., Brown, S., Rompolas, P., Haberman, A.M., et al. (2017). Tissue-scale coordination of cellular behaviour promotes epidermal wound repair in live mice. Nature Cell Biology 2017 19:3 *19*, 155–163. 10.1038/ncb3472.
49. Kennard, A.S., and Theriot, J.A. (2020). Osmolarity-independent electrical cues guide rapid response to injury in zebrafish epidermis. Elife *9*, 1–27. 10.7554/eLife.62386.
50. Shen, K., Jiang, N., Rasmussen, J.P., Clanton, J.A., Rosenberg, M.F., Luedke, K.P., Cronan, M.R., Parker, E.D., Kim, H.-J., Vaughan, J.C., et al. (2019). A conserved morphogenetic mechanism for epidermal ensheathment of nociceptive sensory neurites. 10.7554/eLife.42455.001.
51. Bonacossa-Pereira, I., Coakley, S., Correspondence, M.A.H., and Hilliard, M.A. (2022). Neuron-epidermal attachment protects hyper-fragile axons from mechanical strain. CellReports *38*, 110501. 10.1016/j.celrep.2022.110501.
52. Henson, J.H., Yeterian, M., Weeks, R.M., Medrano, A.E., Brown, B.L., Geist, H.L., Pais, M.D., Oldenbourg, R., and Shuster, C.B. (2015). Arp2/3 complex inhibition radically alters lamellipodial actin architecture, suspended cell shape, and the cell spreading process. *26*. 10.1091/mbc.E14-07-1244.

53. Jelcic, M., Enyedi, B., and Niethammer, P. (2019). Quantitative Imaging of Endogenous and Exogenous H2O2 Gradients in Live Zebrafish Larvae. Methods in Molecular Biology *1982*, 283–299. 10.1007/978-1-4939-9424-3_17.
54. Gault, W.J., Enyedi, B., and Niethammer, P. (2014). Osmotic surveillance mediates rapid wound closure through nucleotide release. Journal of Cell Biology *207*, 767–782. 10.1083/jcb.201408049.
55. Enyedi, B., and Niethammer, P. (2015). Mechanisms of epithelial wound detection. 10.1016/j.tcb.2015.02.007.
56. Diaz, A.C., Schmidt, N.A., Yamazaki, M., Hsieh, C.J., Lisse, T.S., and Rieger, S. (2022). Coordinated NADPH oxidase/hydrogen peroxide functions regulate cutaneous sensory axon de- and regeneration. Proc Natl Acad Sci U S A *119*, e2115009119. 10.1073/PNAS.2115009119/SUPPL_FILE/PNAS.2115009119.SM18.MOV.
57. Korte, B.G., Giese, M.A., Ramakrishnan, G., Ma, S., Bennin, D., Rindy, J., Dewey, C.N., and Huttenlocher, A. (2022). Cell Type-Specific Transcriptome Profiling Reveals a Role for Thioredoxin During Tumor Initiation. Front Immunol *13*. 10.3389/FIMMU.2022.818893.
58. Yoo, S.K., Freisinger, C.M., LeBert, D.C., and Huttenlocher, A. (2012). Early redox, Src family kinase, and calcium signaling integrate wound responses and tissue regeneration in zebrafish. J. Cell Biol *199*, 225–234. 10.1083/jcb.201203154.
59. Yoo, S.K., Starnes, T.W., Deng, Q., and Huttenlocher, A. (2011). Lyn is a redox sensor that mediates leukocyte wound attraction in vivo. Nature *480*, 109. 10.1038/NATURE10632.
60. Niethammer, P., Grabher, C., Look, A.T., and Mitchison, T.J. (2009). A tissue-scale gradient of hydrogen peroxide mediates rapid wound detection in zebrafish. Nature. 10.1038/nature08119.
61. Kirfel, G., and Herzog, V. (2004). Migration of epidermal keratinocytes: Mechanisms, regulation, and biological significance. Protoplasma *223*, 67–78. 10.1007/S00709-003-0031-5/METRICS.
62. Mayor, R., and Etienne-Manneville, S. (2016). The front and rear of collective cell migration. Nature Reviews Molecular Cell Biology 2016 17:2 *17*, 97–109. 10.1038/nrm.2015.14.
63. Olson, H.M., and Nechiporuk, A. v. (2021). Lamellipodia-like protrusions and focal adhesions contribute to collective cell migration in zebrafish. Dev Biol *469*, 125. 10.1016/J.YDBIO.2020.10.007.
64. Yamaguchi, N., Zhang, Z., Schneider, T., Wang, B., Panozzo, D., and Knaut, H. (2022). Rear traction forces drive adherent tissue migration in vivo. Nat Cell Biol *24*, 194. 10.1038/S41556-022-00844-9.
65. Kennard, A.S., and Theriot, J.A. (2020). Osmolarity-independent electrical cues guide rapid response to injury in zebrafish epidermis. Elife *9*, 1–27. 10.7554/ELIFE.62386.
66. Bera, K., Kiepas, A., Godet, I., Li, Y., Mehta, P., Ifemembi, B., Paul, C.D., Sen, A., Serra, S.A., Stoletov, K., et al. (2022). Extracellular fluid viscosity enhances cell migration and cancer dissemination. Nature 2022 611:7935 *611*, 365–373. 10.1038/s41586-022-05394-6.
67. Han, L., Mao, Z., Wu, J., Zhang, Y., and Gao, C. (2012). Influences of surface chemistry and swelling of salt-treated polyelectrolyte multilayers on migration of smooth muscle cells. J R Soc Interface *9*, 3455–3468. 10.1098/RSIF.2012.0546.
68. Sforna, L., Michelucci, A., Morena, F., Argentati, C., Franciolini, F., Vassalli, M., Martino, S., and Catacuzzeno, L. (2022). Piezo1 controls cell volume and migration by modulating swelling-activated chloride current through Ca2+ influx. J Cell Physiol *237*, 1857–1870. 10.1002/JCP.30656.
69. Chen, T., Zhao, H., Gao, L., Song, L., Yang, F., and Du, J. (2019). Hypotonicity promotes epithelial gap closure by lamellipodial protrusion. Prog Biophys Mol Biol *148*, 60–64. 10.1016/J.PBIOMOLBIO.2017.09.021.
70. Sonnemann, K.J., and Bement, W.M. (2011). Wound Repair: Toward Understanding and Integration of Single-Cell and Multicellular Wound Responses. Annu Rev Cell Dev Biol *27*, 237. 10.1146/ANNUREV-CELLBIO-092910-154251.
71. Enyedi, B., Kala, S., Nikolich-Zugich, T., and Niethammer, P. (2013). Tissue damage detection by osmotic surveillance. Nat Cell Biol *15*, 1123–1130. 10.1038/NCB2818.

72. Mendieta-Serrano, M.A., Mendez-Cruz, F.J., Antúnez-Mojica, M., Schnabel, D., Alvarez, L., Cárdenas, L., Lomelí, H., Ruiz-Santiesteban, J.A., and Salas-Vidal, E. (2019). NADPH-Oxidase-derived reactive oxygen species are required for cytoskeletal organization, proper localization of E-cadherin and cell motility during zebrafish epiboly. Free Radic Biol Med *130*, 82–98. 10.1016/J.FREERADBIOMED.2018.10.416.
73. Houseright, R.A., Miskolci, V., Mulvaney, O., Bortnov, V., Mosher, D.F., Rindy, J., Bennin, D.A., and Huttenlocher, A. (2021). Myeloid-derived growth factor regulates neutrophil motility in interstitial tissue damage. J Cell Biol *220*. 10.1083/JCB.202103054.
74. Lam, P.Y., Mangos, S., Green, J.M., Reiser, J., and Huttenlocher, A. (2015). In Vivo Imaging and Characterization of Actin Microridges. PLoS One *10*. 10.1371/JOURNAL.PONE.0115639.
75. Akerboom, J., Chen, T.W., Wardill, T.J., Tian, L., Marvin, J.S., Mutlu, S., Calderón, N.C., Esposti, F., Borghuis, B.G., Sun, X.R., et al. (2012). Optimization of a GCaMP Calcium Indicator for Neural Activity Imaging. Journal of Neuroscience *32*, 13819–13840. 10.1523/JNEUROSCI.2601-12.2012.
76. Huemer, K., Squirrell, J.M., Swader, R., Lebert, D.C., Huttenlocher, A., and Eliceiri, K.W. zWEDGI: Wounding and Entrapment Device for Imaging Live Zebrafish Larvae. 10.1089/zeb.2016.1323.
77. Schneider, C.A., Rasband, W.S., and Eliceiri, K.W. (2012). NIH Image to ImageJ: 25 years of image analysis 10.1038/nmeth.2089.
78. Maeda, H., Fukuyasu, Y., Yoshida, S., Fukuda, M., Saeki, K., Matsuno, H., Yamauchi, Y., Yoshida, K., Hirata, K., and Miyamoto, K. (2004). Fluorescent probes for hydrogen peroxide based on a non-oxidative mechanism. Angew Chem Int Ed Engl *43*, 2389–2391. 10.1002/ANIE.200452381.
79. Cornell, R.A., and Eisen, J.S. (2002). Delta/Notch signaling promotes formation of zebrafish neural crest by repressing Neurogenin 1 function. Development *129*, 2639–2648. 10.1242/dev.129.11.2639.
80. Aitkin M, Anderson D, Francis B, and Hinde J (1989). Statistical Modelling in GLIM (Oxford University Press).
81. Long, J.S., and Ervin, L.H. (2000). Using Heteroscedasticity Consistent Standard Errors in the Linear Regression Model. Am Stat *54*, 217. 10.2307/2685594.

Supplemental Information

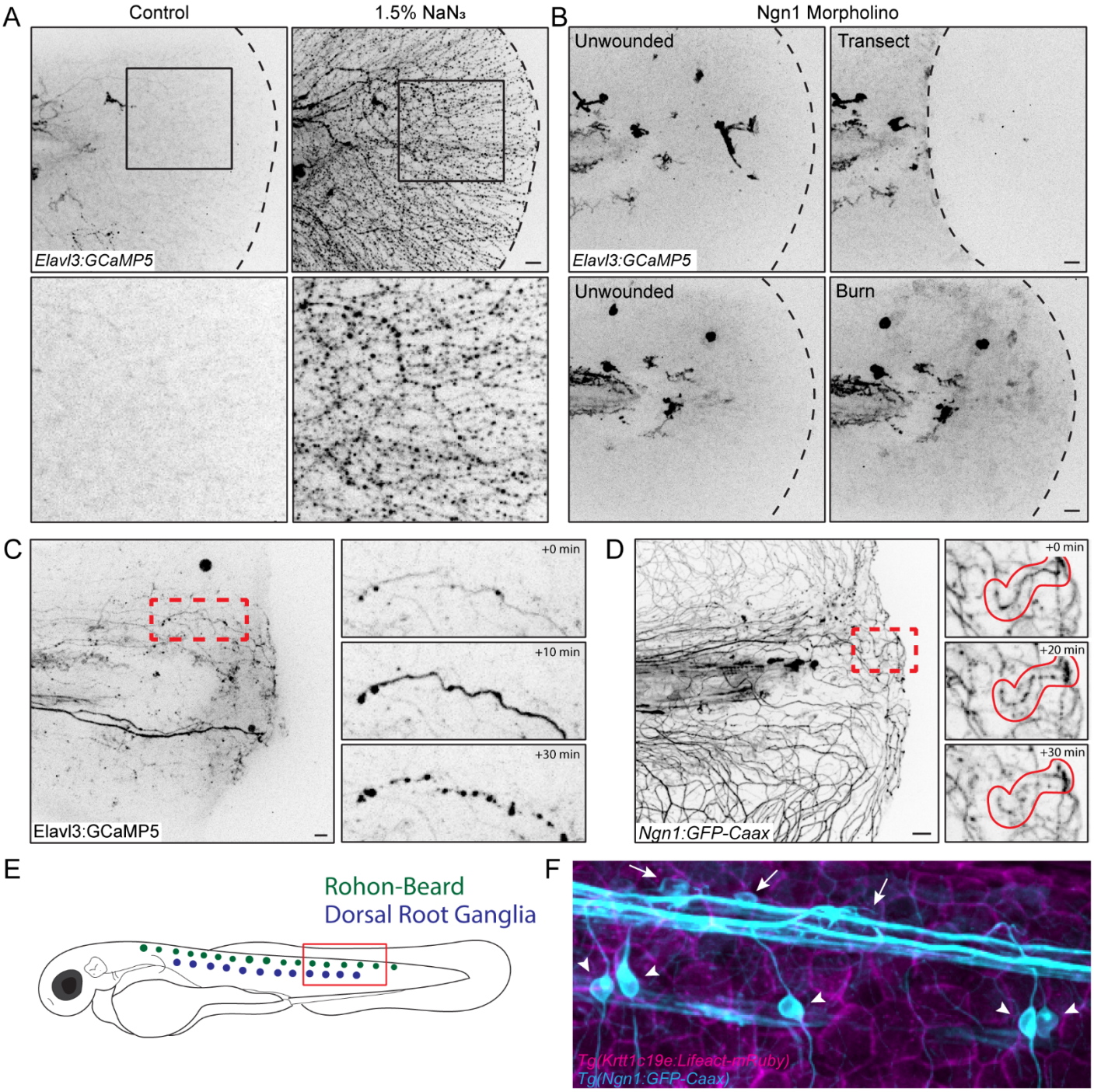

Supplemental Figure 1: Elavl3-GCaMP5 transgenic fish are suitable for visualizing sensory axon damage. (A) Confocal max-projected images of axon damage in *Tg(Elavl3:GCaMP5)* larval zebrafish caudal fins either untreated or 30 minutes post-treatment with the neurotoxin sodium azide (NaN_3, 1.5% final concentration). Sensory neuron damage is indicated by calcium-positive axon fragments (black dots). Dashed black lines denote the fin edge. Black boxes highlight area of inset, shown below. (B) Confocal max-projected

images of *Tg(Elavl3:GCaMP5)* larvae injected with Ngn1 morpholino both before and 5 minutes after the indicated injury. (C) Confocal max-projected images of *Tg(Elavl3:GCaMP5)* larvae taken from a time series. Red dashed box denotes inset area shown on right of a sensory axon fragmenting over a period of 30 minutes. (D) Confocal max-projected images of *Tg(Ngn1:GFP-Caax)* larvae taken from a time series. Red dashed box denotes inset area shown on right of a sensory axon fragmenting over a period of 30 minutes. (E) Schematic of Rohon-Beard (green) and Dorsal Root Ganglia (blue) soma localization in 3 dpf zebrafish. Red box denotes area in which the image shown in F was acquired. (F) Representative confocal max-projected image of intact RB and DRG somas 24 hpw in a *Tg(Ngn1:GFP-Caax); Tg(Krtt1c19e:Lifeact-mRuby)* dual-labeled larva. Arrows denote RB somas, while arrowheads indicate DRG somas. Soma position was unchanged compared to pre-wounding. In all cases, scale bar=20 µm.

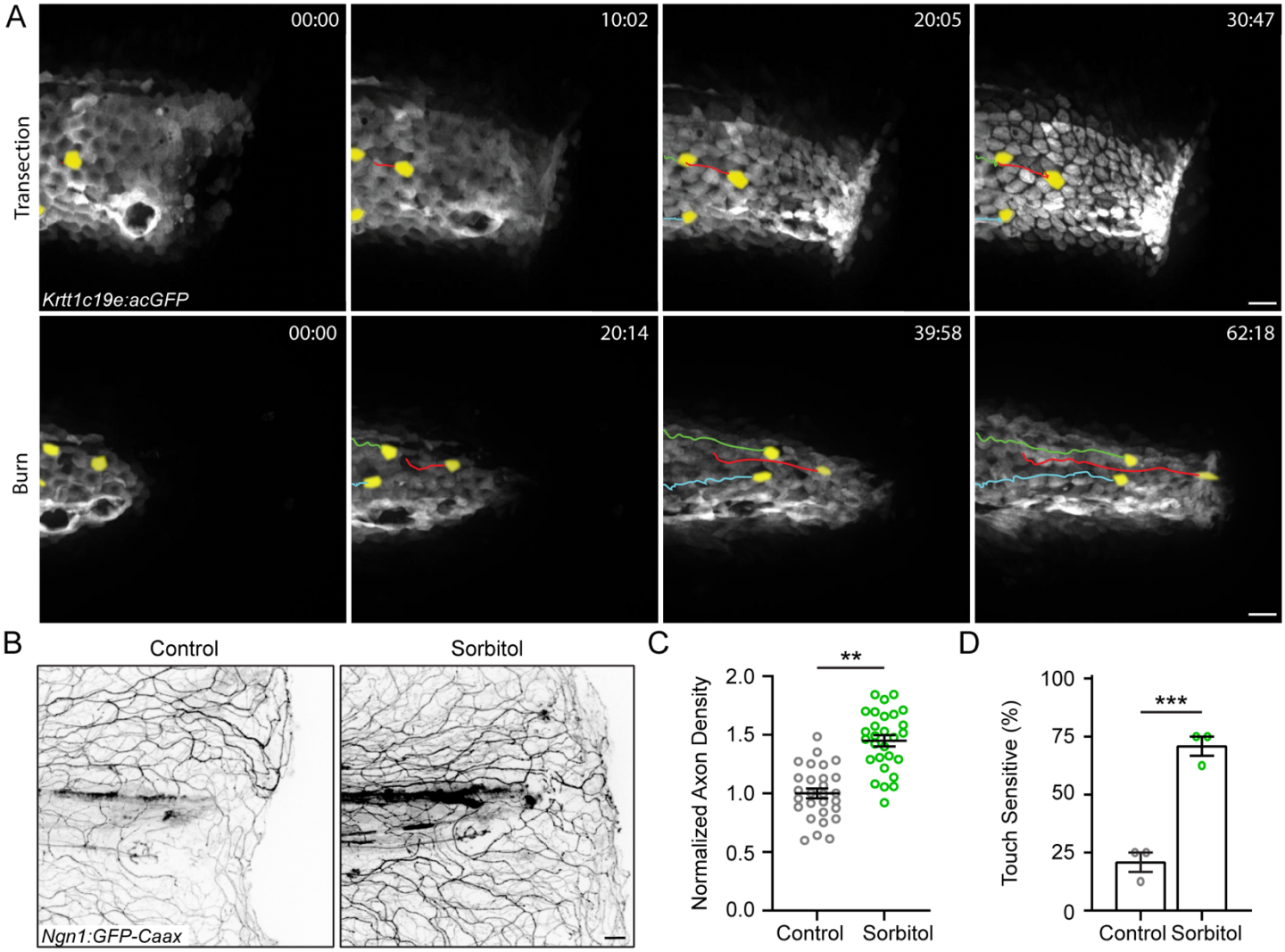

Supplemental Figure 2: Keratinocyte movement after injury and effect of D-Sorbitol on sensory axon regeneration. (A) Confocal time series of basal keratinocyte, *Tg(Krtt1c19e:acGFP),* movement after the indicated injury. Yellow pseudocolored cells highlight keratinocyte displacement. (B) Representative max-projected confocal images of sensory axons in control and isotonic D-Sorbitol treated larvae 24 hpw. (C) Quantification of axon density in wounded tissue 24 hpw. N=28 larvae each from 4 replicates. (D) Quantification of sensory perception 24 hpw. N=24 larvae each collected from 4 replicates. In all cases, scale bar=20 µm. **p<0.01, ***p<0.001.

Supplemental Movie Legends

Supplemental Movie 1: Burn injury induces excessive keratinocyte movement. *Tg(Krt4:UtrCH-GFP)* larvae were injured either by tailfin transection (left) or burn (right). While minimal keratinocyte movement is observed following transection, burn injury results in keratinocyte movement toward the wound edge for approximately 1 hour post-wound. Yellow pseudocolored cells indicate representative keratinocyte movement. Images were collected at 2 frames/min. Scale=20 µm.

Supplemental Movie 2: Epidermal sensory axons move with associated keratinocytes following injury. Basal keratinocyte (magenta), *Tg(Krtt1c19e:Lifeact-Ruby)*, and sensory neuron (cyan), *Tg(Ngn1:GFP-Caax)*, movement was tracked following burn injury. Arrows highlight regions where keratinocyte and sensory axon movement is spatially coincident. Images were collected at 3 frames/min. Scale=10 µm.

Supplemental Movie 3: Tissue movement contributes to axonal damage following burn injury. *Tg(Elavl3:GCaMP5)* larva was burn wounded to track axonal damage, indicated by elevated intracellular calcium (black dots). Damage present at time 0 min is due to the burn wound itself, while new axonal damage coincides with keratinocyte movement. Images collected at 2 frames/min. Scale=20 µm.

Supplemental Movie 4: Wounding in isotonic medium prevents burn-induced keratinocyte movement. Basal keratinocyte, *Tg(Krtt1c19e:acGFP)*, movement was tracked in control (left) and isotonic treated (right) larvae following burn injury. Wounding in the presence of isotonic medium prevents keratinocyte movement associated with burn wounding. Yellow pseudocolored cells indicate representative keratinocyte movement. Images were collected at 2 frames/min. Scale=20 µm.